JGR Oceans

RESEARCH ARTICLE
10.1029/2020JC016643

Barrier Layers in a High-Resolution Model in the Eastern Tropical Pacific

F. M. Bingham[1], Z. Li[2], S. Katsura[3], and J. Sprintall[3]

[1]Center for Marine Science, University of North Carolina Wilmington, Wilmington, NC, USA, [2]California Institute of Technology, Jet Propulsion Laboratory, Pasadena, CA, USA, [3]Scripps Institution of Oceanography, University of California, San Diego, CA, USA

Key Points:

- Salinity barrier layers (BLs) in the eastern tropical North Pacific are characterized using a high-resolution numerical model
- BLs are associated with surface salinity fronts which tilt toward the fresh side at their base
- Vertical circulation combined with surface divergence and convergence are proposed as another formation mechanism for BLs in this region

Supporting Information:

- Supporting information S1
- Movie S1
- Movie S2

Correspondence to:
F. M. Bingham,
binghamf@uncw.edu

Citation:
Bingham, F. M., Li, Z., Katsura, S., & Sprintall, J. (2020). Barrier layers in a high-resolution model in the eastern tropical Pacific. *Journal of Geophysical Research: Oceans*, *125*, e2020JC016643. https://doi.org/10.1029/2020JC016643

Received 23 JUL 2020
Accepted 11 NOV 2020

Abstract This study examines salinity barrier layers (BLs) in the eastern tropical North Pacific in the region of the Salinity Processes in the Upper ocean Regional Studies-2 field campaign. We utilize a high-resolution numerical model to study BLs and their relationship to frontal features and small-scale ocean variability, focusing on two specific events. One is associated with a large outbreak of BL presence near 7°N along 125°W. The other is a relatively isolated but persistent BL that forms near 13°N, again along 125°W. In both cases we find that the BL is proximate to a salinity frontal feature in which isohalines tilt toward the fresh side of the front at its base. The BLs studied are associated with divergent flow at the surface on the fresh side of the front and convergent flow on the salty side. Tilting of the front is invoked to explain this, with an additional mechanism involving a vertical circulation which causes the base of the front to tilt preferentially.

Plain Language Summary Salinity barrier layers (BLs) are common in the eastern tropical North Pacific (ETP) ocean. They consist of a surface mixed layer that is homogeneous in temperature, but with a high salinity layer at the base. They may play an important role in regulating the transfer of heat, momentum, and freshwater across the ocean surface and from there into the interior. This study examines BLs in the ETP in the region of the Salinity Processes in the Upper ocean Regional Studies-2 (SPURS-2) field campaign using a high-resolution numerical simulation. SPURS-2 took place in 2016–2017 and was designed to study processes connecting salinity and rainfall in the ETP in the vicinity of the intertropical convergence zone. Two specific examples of BLs are studied. In one, there is a large outbreak of such layers throughout the ETP along a large-scale sea surface salinity (SSS) front. In the other example, the BL was an isolated feature associated with another sharp SSS front. So frontal features are an important part of the process of BL formation. In addition, we find surface flow which converges toward the front on the salty side and diverges away from it on the fresh side. BL formation at the front is a result of the front tilting away from the vertical, and in the case of the fronts studied here, that tilting is concentrated at the front's base. It is also likely associated with vertical circulation on either side of it.

1. Introduction

Barrier layers (BLs) are areas in the upper ocean where the surface mixed layer as defined by temperature is greater than that as defined by density due to the presence of salty water at the base of the mixed layer. They have been observed in the ocean since their discovery about 30 years ago (Godfrey & Lindstrom, 1989; Lukas & Lindstrom, 1991). BLs have been found in a diverse set of contexts (Sprintall & Tomczak, 1992; de Boyer Montegut et al., 2007), most especially in the tropics and at high latitudes, and are an important part of upper ocean dynamics in these areas (Roemmich et al., 1994; Vialard & Delecluse, 1998a). In the tropics in particular, they are thought to modulate air-sea interaction by creating a layer of insulating stratification, which can magnify the impact of heat and/or freshwater flux at the surface (Maes et al., 2002, 2005). They also act to suppress entrainment cooling at the base of the mixed layer, since water in the mixed layer is at the same temperature as water below it (Godfrey & Lindstrom, 1989; Vialard & Delecluse, 1998b).

BLs have been extensively studied in the western Pacific, but not as much in the eastern Pacific. Conditions are different in the eastern part of the basin where the forcing is more seasonal. Katsura and Sprintall (2020; henceforth "KS20") have shown that BLs are ubiquitous in the eastern tropical North Pacific (ETP) under the intertropical convergence zone (ITCZ; Qu et al., 2014). Their presence is highly seasonal, with

maximum likelihood and thickness in the summer and fall (de Boyer Montegut et al., 2007). The KS20 study was a climatological seasonal one based on sparse Argo data, so BLs were only discussed on a monthly time scale. KS20 attribute the common presence of BLs in this region to convergent Ekman transport driven by wind stress curl. The Ekman convergence creates mixed layer salinity fronts, which then tilt due to instability and shear between the surface and the base of the mixed layer. This process of tilting was first proposed by Cronin and McPhaden (2002; henceforth "CM02") as one potential mechanism for BL formation. KS20's conclusion is congruent with Sato et al. (2004, 2006) and Katsura et al. (2015), who all emphasized the role of sharp small-scale salinity fronts and subduction of high salinity water in the tropical and subtropical ocean. However, the conclusions of KS20 and those of Sato et al. (2006) are based on Argo data which are relatively sparse in space and time. In particular, KS20 cannot co-locate the BLs relative to the concurrent position of the North Equatorial Counter Current or any property front associated with the circulation system, nor do they shed any light on what specific dynamics may be occurring at the front associated with BL formation. Indeed, it is difficult to obtain the direct measurements of the three-dimensional circulation and air-sea interaction that are needed to determine the mechanisms responsible for BL formation using an in situ dataset.

Katsura et al. (2020) looked in more detail at BL and temperature inversion formation using the higher resolution Salinity Processes in the Upper ocean Regional Studies-2 (SPURS-2) in situ dataset. They reached a similar conclusion as KS20, that BLs form as a result of tilting of mixed layer fronts. Additionally, they surmise that BLs form in a patchy and intermittent manner on fast time scales and that surface geostrophic flow and Ekman flow play important roles in causing the tilting of frontal isohalines—where BL formation occurs. However, Katsura et al. (2020) is based on shipboard observations, so temporal changes in BLs cannot be described even though synoptic BL features were observed.

The ETP is the location of the seasonal extension of the ETP fresh pool (Alory et al., 2012; Melnichenko et al., 2019), a low surface salinity feature which extends westward from the coast of Central America. It reaches its maximum extent in the October/November period, reaching out to ∼160°W, as defined by the 34 isohaline, with minimum extent in January/February at ∼125°W. Its meridional extent, again defined by the 34 isohaline, is about 10° in the mean between about 5–15°N (Guimbard et al., 2017; Fiedler & Talley, 2006). At the southern edge of this fresh pool extension is a surface front separating the relatively fresh eastern Pacific water from higher salinity surface water found at the equator. This front forms in January near ∼3°N, migrates to the north over the course of the year, and dissipates in the months of January-February after reaching a maximum latitude of about 12°N (Yu, 2015). In the October-November, period it is generally found around 6–7°N, which is one location where the present study will focus. The ETP is unique due to the intense currents, strong fronts, dominance of Ekman transport, and shallow mixed layers that are present. These all likely point to the CM02 tilting mechanism as the most important one for BL formation. BLs in the ETP are generally thinner than in the western Pacific (Fiedler & Talley, 2006). The ETP is also a site of intense rainfall (Schanze et al., 2010). However, according to KS20, rainfall and BLs do not generally coincide, meaning that rainfall may not be an important mechanism contributing to the formation. Thus, we would like to look at the tilting mechanism in the ETP in more detail.

Using a numerical model, we can focus in on the mechanisms responsible for BL formation, and examine how or whether the BL formation is related to three-dimensional frontal structures and their temporal evolution. As stated by Tanguy et al. (2010), a complete understanding of BL formation requires information "on the three-dimensional structure of the upper ocean, T, S, velocity, vertical shear, local surface forcing and turbulent mixing." BL formation in numerical models has been studied by Veneziani et al. (2014) in the South Atlantic, using the same model formulation we use here, though configured specifically for that different region. They emphasized the importance of advection, and, importantly, of the influence from submesoscale processes at 1–9 km spatial scales and their impact on vertical transport of heat and salt. The ETP was the location, in 2016–2017, of the SPURS-2 field campaign (Lindstrom et al., 2019 and references therein), carried out to study the impact of rainfall on the upper ocean salinity field, and the creation of the Pacific basin-wide low sea surface salinity (SSS) feature (e.g., Schanze et al.., 2010). Associated with the field campaign, there was an effort to simulate the dynamics in a regional ocean model based on the Regional Ocean Modeling System (ROMS; Li et al., 2019; henceforth "Li19"; Shchepetkin et al.., 2011).

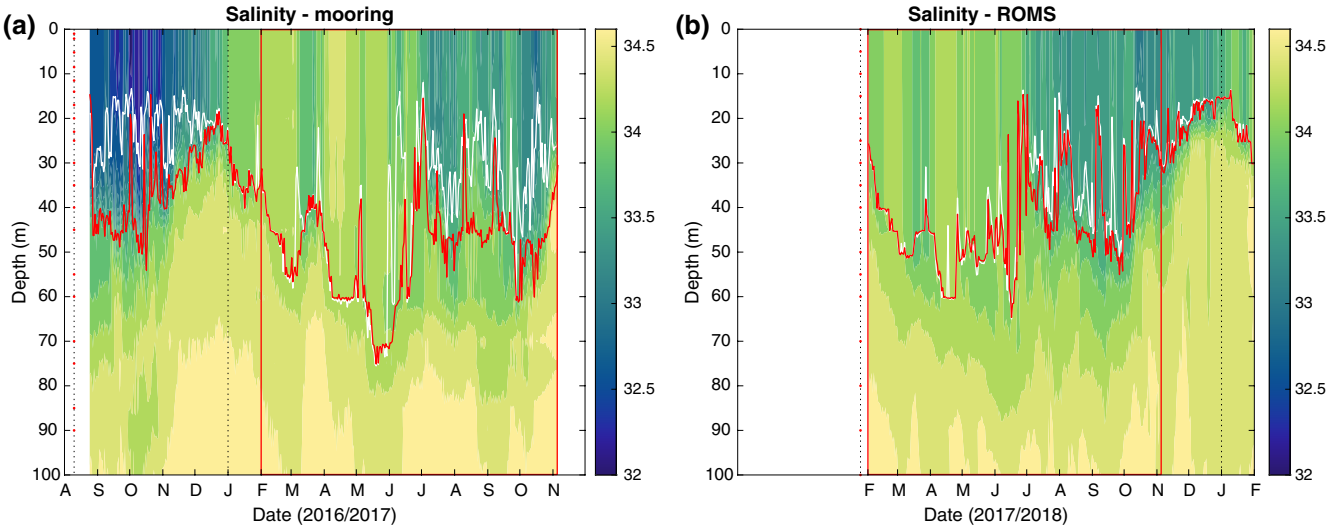

Figure 1. Time series of salinity versus depth observed at (a) the SPURS-2 central mooring (10°N, 125°W) (Farrar, 2019) and from (b) the corresponding grid cell in the ROMS simulation. ILD is in white and MLD in red. The difference between them is the BLT. Color scales are at right for each panel. Also note these two panels do not cover the same periods. Mooring salinity covers the period August 2016–November 2017, whereas the ROMS salinity is computed over February 2017–January 2018. A red box in each panel outlines the overlapping time period, February–November 2017. At the left of each panel are vertically arranged red dots showing the locations of the mooring instruments above 100 m in panel (a) and the ROMS interpolated vertical levels above 100 m in panel (b). BLT, barrier layer thickness; ILD, isothermal layer depth; MLD, mixed-layer depth; ROMS, Regional Ocean Modeling System; SPURS-2, Salinity Processes in the Upper ocean Regional Studies-2.

In this study, we study BL formation in a couple of individual events within the high-resolution ROMS daily output. The ROMS output displays BLs in the ETP, which can be related to surface circulation, surface convergence, salinity, winds, and freshwater forcing from the atmosphere. ROMS allows us to examine the processes involved in BL formation at a scale and level of detail that is not possible with in situ data. Also, while BLs have been frequently studied in the western Pacific, less is known about their characteristics and formation mechanisms in the ETP where forcing is much more seasonal as it is aligned with the seasonal march of the ITCZ. The choice of events to study was somewhat arbitrary. We wanted to look at one instance that could be directly compared to data collected during the SPURS-2 field campaign and another event that was relatively isolated and long-lived. These events are not necessarily typical. However, by studying a couple of individual instances, we may be able to infer more broadly about how BLs relate to the dynamics of the ETP fresh pool and its seasonal extension across the Pacific.

2. Data and Methods

2.1. ROMS Simulation

The ROMS simulation (Li, 2020) uses data assimilation to constrain the large-scale and large mesoscale circulations as a method for more realistically reproducing BL formation. The model is nested in three levels, 9, 3, and 1 km (see Figure 2 in Li19). We use the 3 km, middle level, with daily average output. In the vertical, the model has 52 levels. To effectively resolve dynamical processes associated with BL formation 22 of those are within the top 100 m, with the topmost level at 1 m. Model output was interpolated onto a set of standard levels to do the calculations discussed and displayed in this study (Figure 1b). The model covers the time period February 1, 2017–January 31, 2018, whereas the SPURS-2 field campaign went from late August 2016 to early November 2017. Thus, the model and field campaign overlap for about 9 months of 2017 (Figure 1).

The atmospheric forcing for ROMS is derived from the 18 km resolution National Centers for Environmental Prediction Global Forecast System (GFS) operational atmospheric model output. A bulk flux formula (Fairall et al., 2003) is used to calculate the forcing. The inputs include 3-hourly atmospheric fields of 10-m

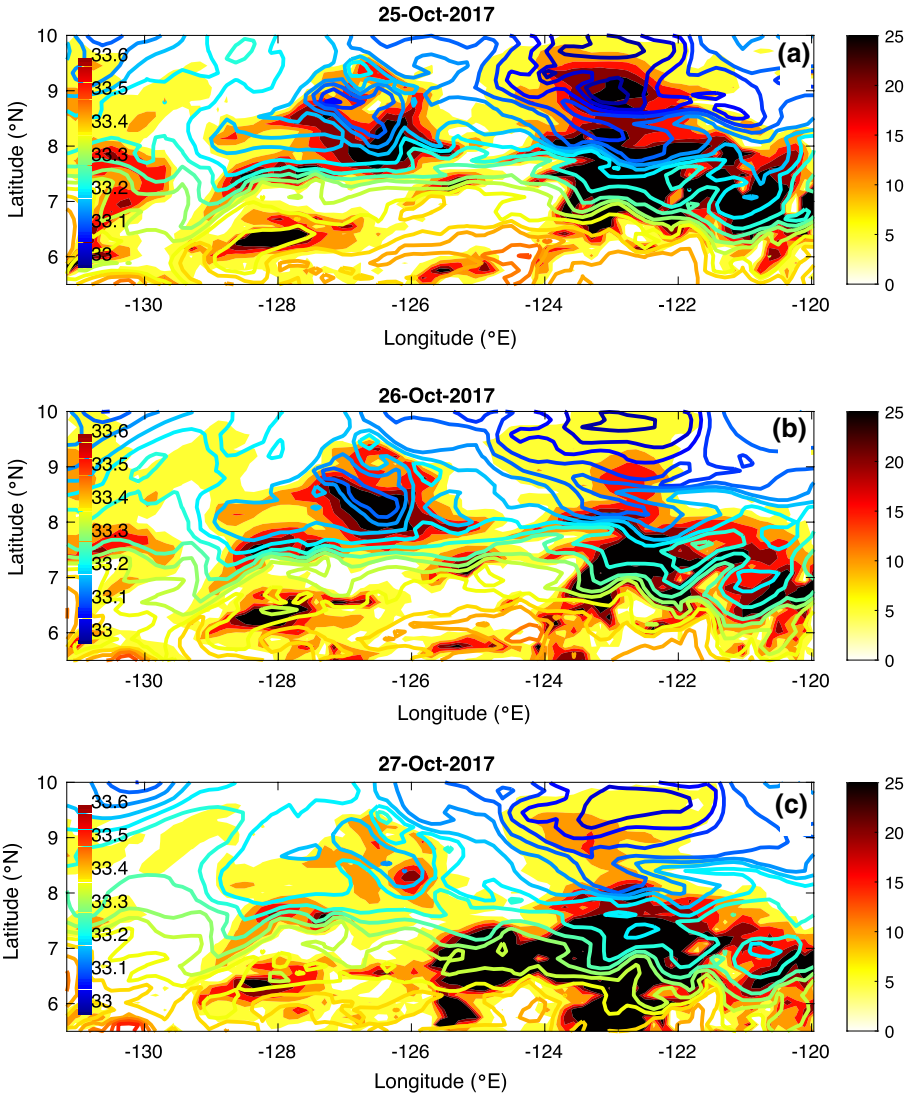

Figure 2. Contours: SSS with color scale at left. Shading: BLT in meters with color scale at right. (a) 25-October. (b) 26-October. (c) 27-October. BLT, barrier layer thickness; SSS, sea surface salinity.

wind speed and direction, net shortwave radiation, downward longwave radiation, 2 m air temperature, 2 m relative humidity, and precipitation. Rainfall in this region tends to come in very heavy and patchy downpours whose sizes are on the order of a few km (Rutledge et al., 2019; Thompson et al., 2019). The 18 km resolution of the model forcing does not allow one to distinguish these individual rain events, and thus changes to SSS associated with convective rainfall are not represented in the ROMS simulation.

The model assimilates a number of datasets. One of these is the monthly average data from version 4 of the Met Office Hadley Centre "EN" series (Good et al., 2013). This monthly dataset constrains three-dimensional T/S fields on spatial scales larger than 400 km and thus is used to reduce model bias. Another assimilated dataset is the gridded Archiving, Validation and Interpretation of Satellite Oceanographic data (AVISO) sea surface height product. This product has a grid of 0.25°, but the effective resolution is about 300 km (Pujol et al., 2016). Satellite sea surface temperature (SST) measurements from the Advanced Microwave Scanning Radiometer-2 (AMSR-2), a passive microwave radiometer flying on NASA's Aqua satellite, are also assimilated. The AMSR-2 SST has a resolution of 0.25°. Using the multiscale scheme as described in Li et al. (2015, 2019), the data assimilation is configured to primarily constrain eddies and circulation

with spatial scales larger than 300 km. There are no SPURS-2 in situ observations assimilated in this 3 km model domain.

Real-time forecasts of the modeling system during the SPURS-2 field campaign have been encouraging. As presented in Li19, a range of evaluations showed the modeling system predicted the time evolution of the mesoscale circulation compared to measurements of sea surface height (SSH), SST, and surface currents. For example, the 2-day SSH forecast had a spatial correlation larger than 0.9 and a root-mean-square error (RMSE) of less than 4 cm against the AVISO gridded data product on a daily basis, and the model SST forecast had a RMSE of 0.6°C against observations from as many as 130 drifters. The vertical T/S profiles are comparable to the observed. As such, we are convinced that the BLs that the model produces essentially represent the same dynamical processes that are responsible for the generation of the observed BLs.

From the model output, we computed such quantities as divergence and vorticity. Isothermal layer depth (ILD) and mixed-layer depth (MLD) were determined using the method of de Boyer Montegut et al. (2007). In that study, the ILD (their "$D_{T\text{-}02}$") is defined as the depth where potential temperature is greater than that at a reference depth by 0.2°C. The MLD (their "D_{σ}") is the depth where "the potential density ... has increased from that at the reference depth by a threshold ... equivalent to the density difference for the same temperature change at constant salinity." They use a reference depth of 10 m, but here we use 0 m. BL thickness (BLT) is the difference between ILD and MLD when that difference is greater than zero.

2.2. In Situ Data

Brief use is made in this study of data (Farrar, 2019) from the SPURS-2 central mooring (Figure 1a). See Farrar and Plueddemann (2019) for a description of the methods associated with this dataset.

Brief use is also made below of underway conductivity-temperature-depth (uCTD) data from SPURS-2 (Sprintall, 2019a, 2019b). These data have vertical resolution of about 6 m. For the section we display below, the horizontal resolution is about 0.1° along-track (Katsura et al., 2020).

3. Results

In the supporting information we include an animation of BLT within the model during the SPURS-2 period along with SSS (Movie S1). Thick BLs are often generated within eddies (e.g., February 8, 2017–February 20, 2017 at 12.5°N, 124°W) or across strong fronts (e.g., May 12, 2017–May 22, 2017 at 13°N, 125°W). These BLs can persist for days or weeks, or appear and disappear in a day or two (e.g., July 31, 2017–August 1, 2017). They can be isolated in time and space, or be ubiquitous throughout a large part of the domain shown (e.g., June 29, 2017). BLs appear in the model output, but they are not generally as thick or persistent as those in the in situ data. This is evident through a comparison (Figure 1) between model output and observed T/S data from the SPURS-2 central mooring. Note the ubiquitous presence of 20–30 m thick BLs in late summer and fall in the mooring data which are either absent or more sporadic in the ROMS simulation.

3.1. October Event

Thick BLs are present intermittently along an SSS front south of 10°N that persists for much of October and November (Movie S1). Figure 2 shows this for a 3-day period near the end of October. A strong relationship is seen between SSS fronts and BLs. Thick BLs are often present on the fresh side of a front. Examples are seen at 7.5°N, 128°W, or 7°N, 123°W on all 3 days. Some of these features are persistent over the 3-day period (e.g., 7.5°N, 128°W). Others evolve rapidly, either dissipating (e.g., 8.5°N, 127°W), or suddenly appearing (e.g., 6.5°N, 125°W). It's this last feature that we will now study in detail as it develops.

On October 27, 2017 there is a very thick BL around 6–7°N from 126°W to 120°W (Figure 2c). It does not seem to be connected to BLs seen further west in the prior days, as the current speeds are not fast enough for advection to work. Much of the model domain south of 8°N on 27-October shows BLs that are >25 m thick. These thick BLs are associated with a complex SSS front that snakes through the region from (6°N, 120°W)

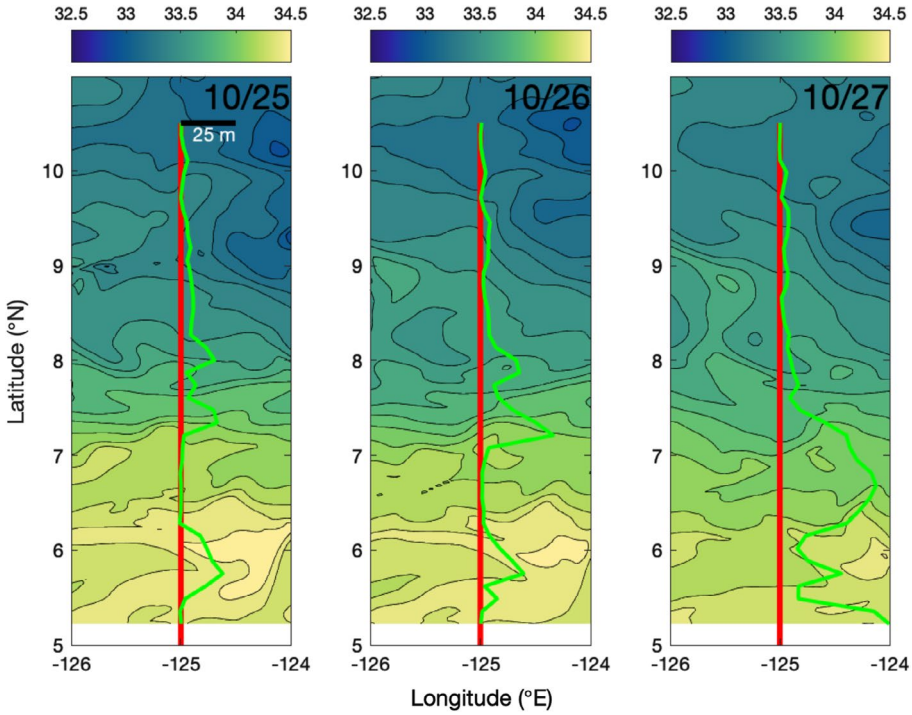

Figure 3. SSS from the ROMS domain on (left panel) 25, (center panel) 26 and (right panel) October 27, 2017. Color scale is at the top. Red line is along 125°W. The thick green line represents the BLT at 125°W at a given latitude, where zero BLT is the red line and 25 m BLT is indicated by the scale bar at 10.5°N in the left panel. BLT, barrier layer thickness; ROMS, Regional Ocean Modeling System; SSS, sea surface salinity.

to (7°N, 129°W) (Movie S1, Figure 2c) on this day. On 27-October, the BL is centered at about 6.75°N, but is relatively thick from 6°N to 7.5°N along 125°W (Figure 3 right panel). What is clear from the SSS is the low salinity water spreading to the south during the prior 2 days. The SSS front relaxes and becomes more diffuse at 125°W as seen in the contrast between 26 and 27 October as seen in Figures 2 and 3 and Movie S1. Water in the vicinity of the thick BL is much fresher on 27-October than the two previous days (Figures 3a and 3b) when no or minimal BLs existed.

The ocean current vectors (Figure 4) on 27-October show water flowing eastward throughout the entire domain. The thick BL of 27-October is associated with the sharply decreased SSS brought about by advection and the southward motion of a SSS front. A convergent feature is evident in the northern part of the region of thick BLs around 7°N (Figure 4 right panel). Just to the south of this convergent feature is an area of divergence near the center of the area of thick BL. This same convergent feature has migrated over the previous 2 days when it is also associated with thick BLs, although not as thick as on 27 October (e.g., 7.2°N on 26 October). So thick BL formation in this instance appears to be associated with surface convergence and divergence.

The thick BLs on all 3 days are associated with areas of intense surface divergence and convergence culminating on 27 October (Figure 5 right panel). The thickest BLs are associated with surface divergence on the fresh side of the front and there is some indication that surface convergence is associated with reduced BLT (e.g., 5.5°N and 6°N on 27 October). There are also places where thick BLs are associated with alternating surface convergence and divergence, for example around 6°N on 25 October and 7.25°N on 26 October. It should be noted here that we have examined other variables such as SST and vorticity over large scales. Divergence seems to have the most consistent relationship with BLs such as is seen in Figure 5.

The precipitation forcing the model is very small on 27 October and far removed from where the thick BLs are formed (Figure 6, right panel). An area of heavy precipitation is located at (7.75°N, 125.5°W) on 26 October which may have had an influence on the thick BLs at 6.75°N the following day, though this is not

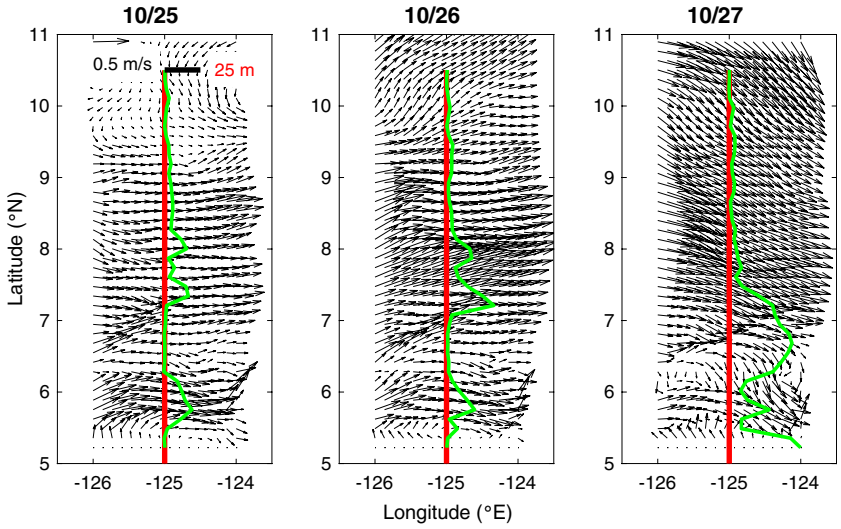

Figure 4. As in Figure 3, but for current velocity vectors. A scale arrow is at the top left in the left panel.

obvious from the SSS shown in Figure 3. Note that this map of precipitation is very smooth compared to the ones of Thompson et al. (2019) and Rutledge et al. (2019) from the same region and time period, and has larger scales of variability.

Wind speed undergoes a rapid change from 25–26 October to 27 October (Figure 7). On 27 October, the winds were nearly calm, whereas in the region of thick BL the winds were up to 8 m s^{-1} on the previous 2 days. The winds on 25–26 October were mainly out of the south (not shown). Perhaps the sudden change in the winds allowed low SSS water at the surface to drift southward after the change.

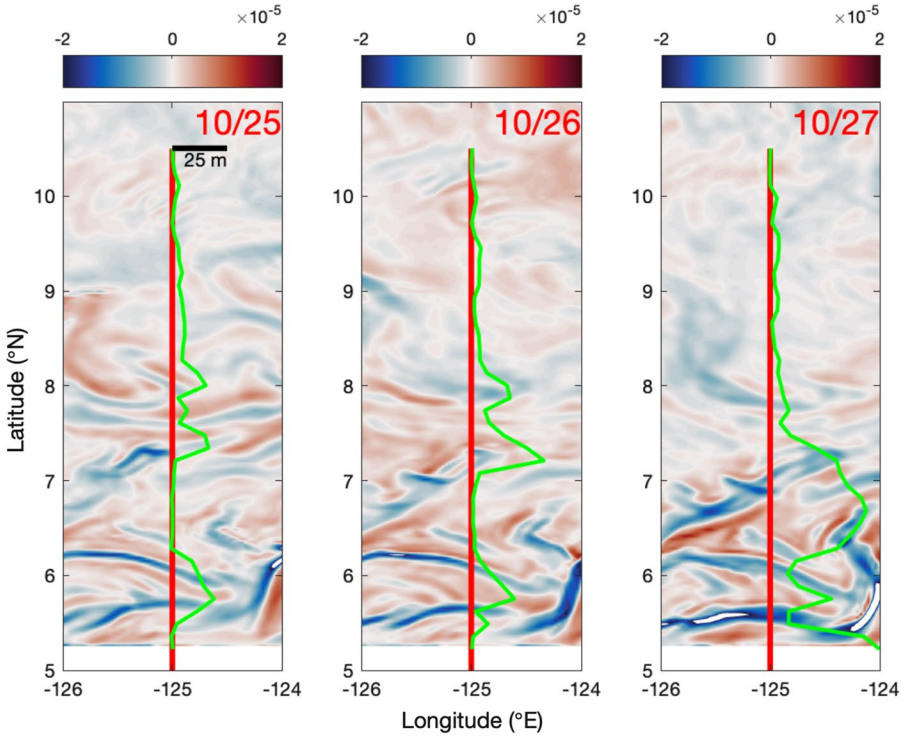

Figure 5. As in Figure 3, but for horizontal divergence. Color scale is at the top of each panel in units of s^{-1}.

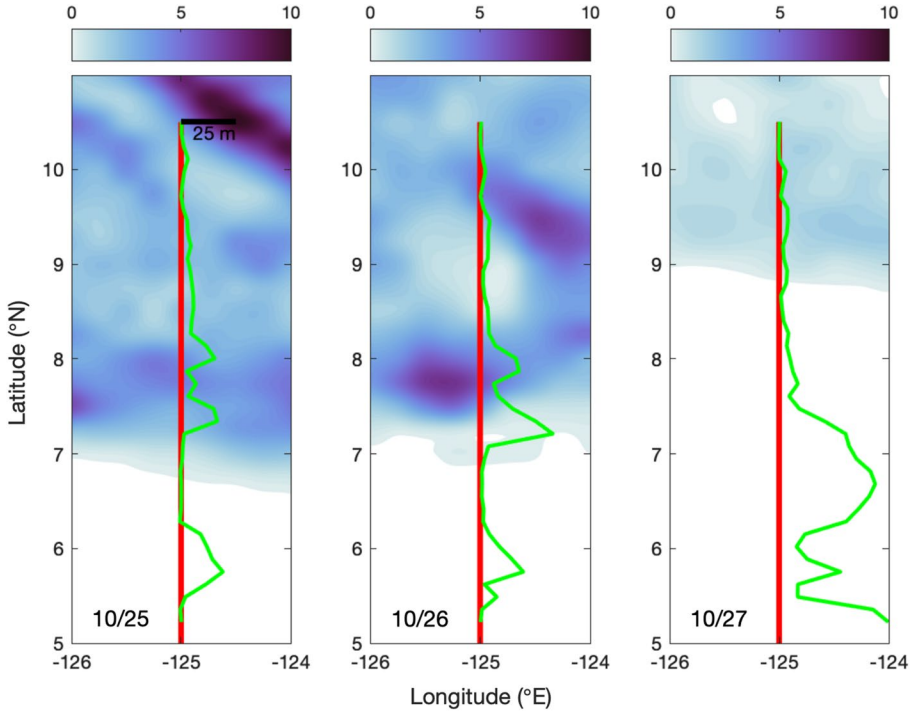

Figure 6. As in Figure 3, but for daily average precipitation rate. Color scale is at the top for each panel in units of mm hr^{-1}.

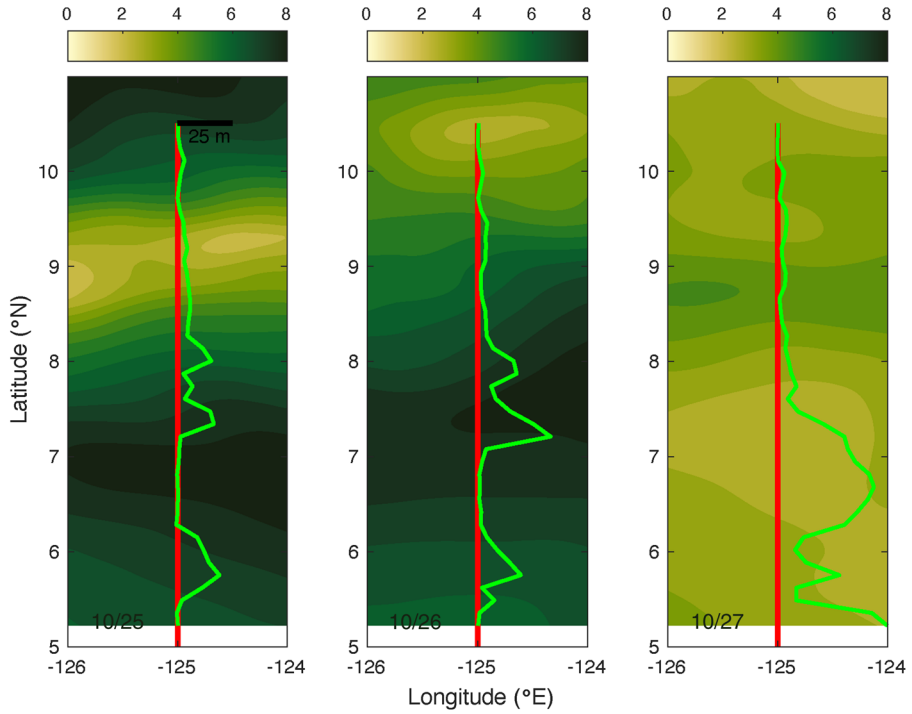

Figure 7. As in Figure 3, but for surface wind speed. Color scale is at the top for each panel in units of m s^{-1}.

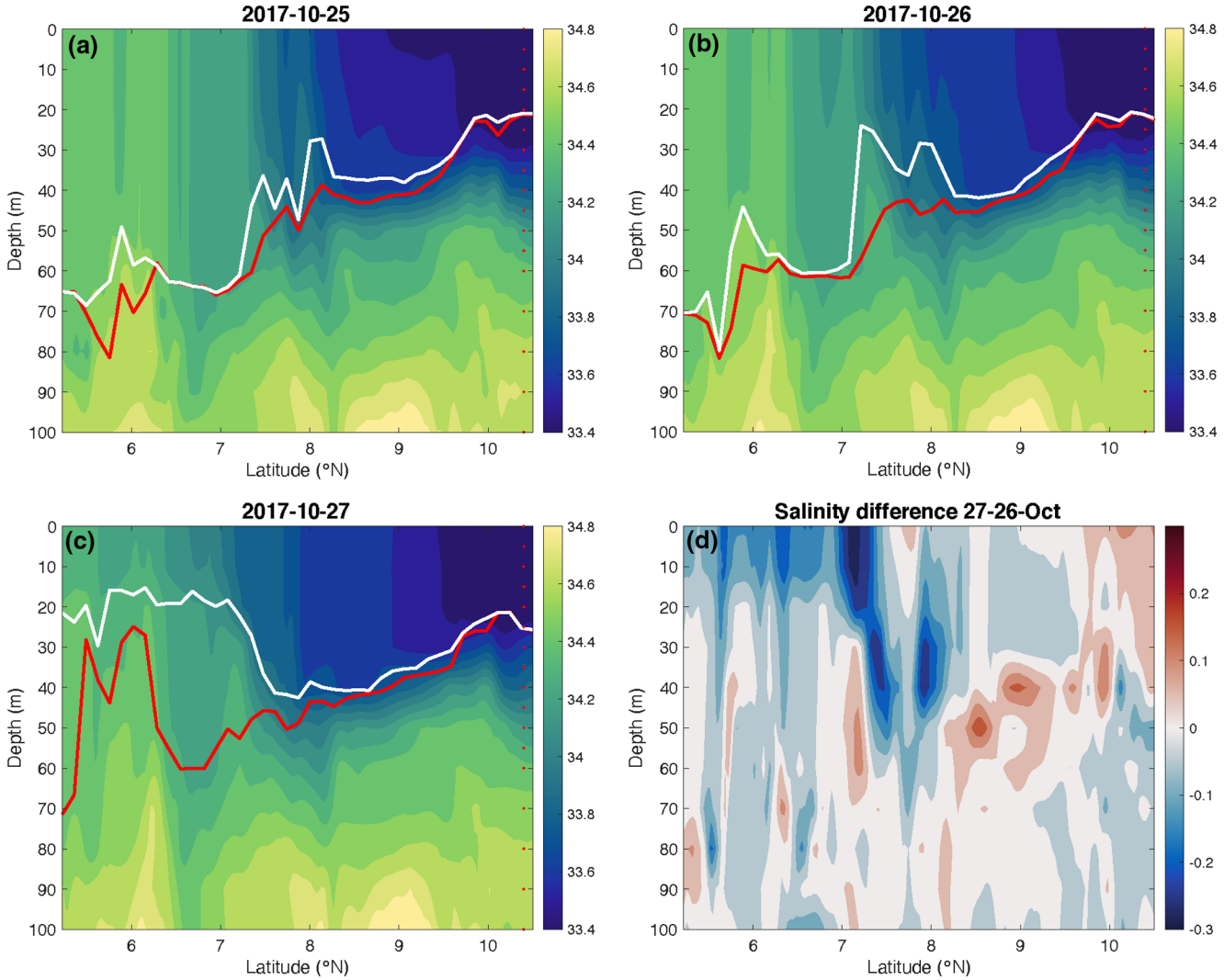

Figure 8. ROMS Salinity sections along 125°W for (a) 25 October, (b) 26 October, and (c) 27 October. Each panel represents a daily average centered at 1500 Z each day. Color scales are at right. Small red dots near the right side of panels (a–c) are the locations of the model levels used in this study. Thick red line is the ILD, while thick white line is the MLD. (d) Difference between panels (c) and (b). ILD, isothermal layer depth; MLD, mixed-layer depth; ROMS, Regional Ocean Modeling System.

A meridional section along 125°W (Figure 8) shows fresh surface water spreading across the area between 6 and 7°N and the generation of a thick BL. On 25 and 26 October, there is a thin BL between 7 and 8°N (Figures 8a and 8b). By 27-October, relatively fresh surface water had spread southward to around 6°N (Figure 8c). This spreading occurred in the upper 20 m as evident in the large salinity difference shown in Figure 8d. The spreading left a thick BL between 6.25 and 7.5°N. South of there, between 26 and 27 October, the ILD shoaled from 60 to 30 m. What we see here is somewhat like the tilting of isohalines posited by CM02, but it is not exactly the same. In the main, the isohalines tilt during the days shown, but the tilting goes on mostly below 20 m depth. That is, the base of the isohalines tilts, but the upper part remains vertical. The salinity front at 7.5°N relaxes and spreads southward. CM02 implied that BLs are generated by current shear which causes the tilting (see their Figure 1). A complicating fact is that the zonal flow is much stronger than meridional. Perhaps in this case the tilting is not caused by cross-front vertical shear, but by some other mechanism.

October 2017 coincided with one of the two main SPURS-2 cruises. A uCTD section to ~250 m was obtained along 125°W from 10.5 to 5°N on 26–28 October (Figure 9). This uCTD section also showed that a thick BL existed, but it was much thicker (~50 m) and more extensive (from 9° to 6°N) than that produced in the

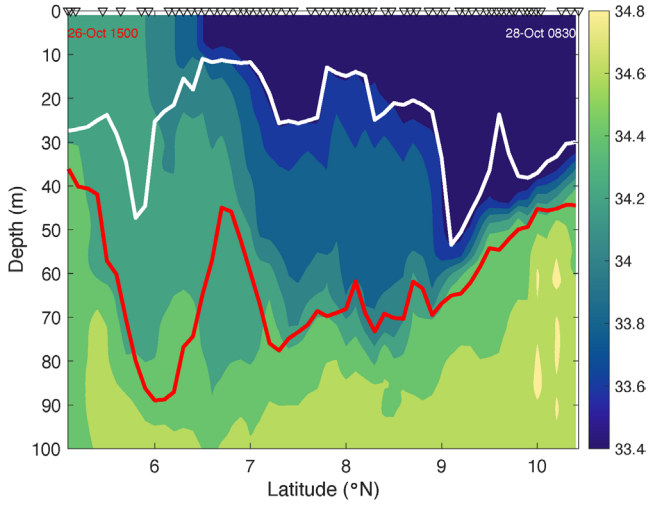

Figure 9. Salinity section from uCTD data (Sprintall, 2019a, 2019b) along 125°W collected on the R/V Roger Revelle, 26–28 October 2017. Color scale is shown at right. Thick red line is the ILD, while thick white line is the MLD. Vertical resolution of uCTD data is ~6 m. Dates and times shown at the top left and right are for the first and last casts. Thus, the section data were collected as the ship moved from south to north and took about 1.7 days to complete. Inverted triangles at the top are the locations of the casts—there were 62 of them. ILD, isothermal layer depth; MLD, mixed-layer depth, uCTD, underway conductivity-temperature-depth.

ROMS output (Figure 8). There is as salinity front at the surface near 6.5°N. We also see the same configuration of the front, vertical isohalines at the surface and tilted ones below it as was observed for the model. The difference here is the that BL is much thicker in the uCTD data and the part of the water column with vertical isohalines much thinner. Katsura et al. (2020) show a similar section from a few days later, 3–5 November.

It is clear from Figures 4 and 5 that the presence of BLs is strongly related to surface horizontal divergence/convergence. Thus, because divergence and convergence are usually accompanied by vertical motion, it is likely related to vertical processes such as vertical flows, mixing, and entrainment. The vertical velocity along 125°W (Figure 10) shows alternating bands of strong upward and downward flow in the mixed layer south of 7.5°N on 27 October. As expected, these bands are directly related to the maps of surface divergence (Figure 4), upward flow occurs where there is surface divergence and downward flow where there is convergence. The strong flow ceases at the base of the mixed layer, except for one band of downward flow at 5.6°N. For the most part, where the BL is thickest, the flow is upward. Where vertical velocity is minimal, north of 8°N, BLs are thin to nonexistent. This pattern is repeated at 5.5–6°N and 7.5–8°N on the previous day (Figure 10a).

3.2. May Event

Between May 7 and 26, 2017, especially starting around May 9, a BL developed across a north-south oriented front between 12 and 13°N near 125°W (Movie S1). This BL reached a maximum BLT of more than 25 m and persisted for more than 2 weeks within the front, eventually migrating northward to turn to an east-west orientation further north before dissipating by May 30. The BL is clearly evident in the horizontal plan view (Figure 11a, Movie S2). Similar to the October event, there is tilting of isohalines (Figure 11b). The BL is situated on the low salinity side of the front at 125°W, with fresher water to the east. The front is tilted in the vertical, but not uniformly. All of the tilting occurs at the base of the front between 30 and 60 m depth, similar to that found in the October event (Figure 8c). The horizontal velocity field shows a tilting convergent strip that is close to the

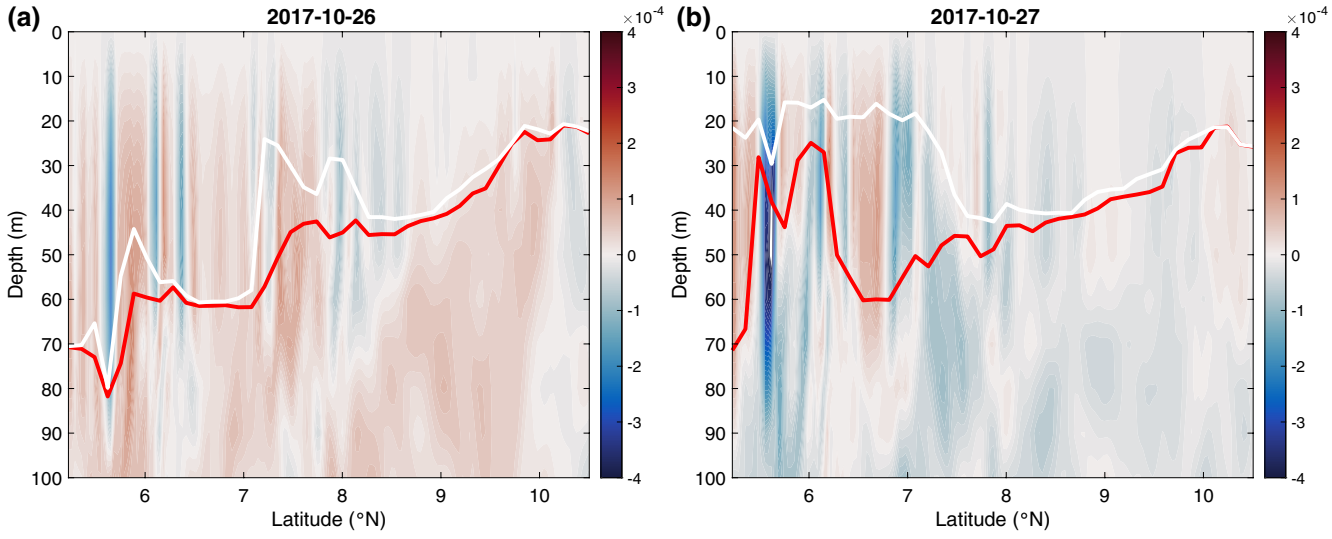

Figure 10. Vertical velocity sections along 125°W for (a) 26 and (b) 27 October. Color scales (in m/s) are at right. Red colors are upward and blue downward. Thick red line is the ILD, while thick white line is the MLD. ILD, isothermal layer depth; MLD, mixed-layer depth.

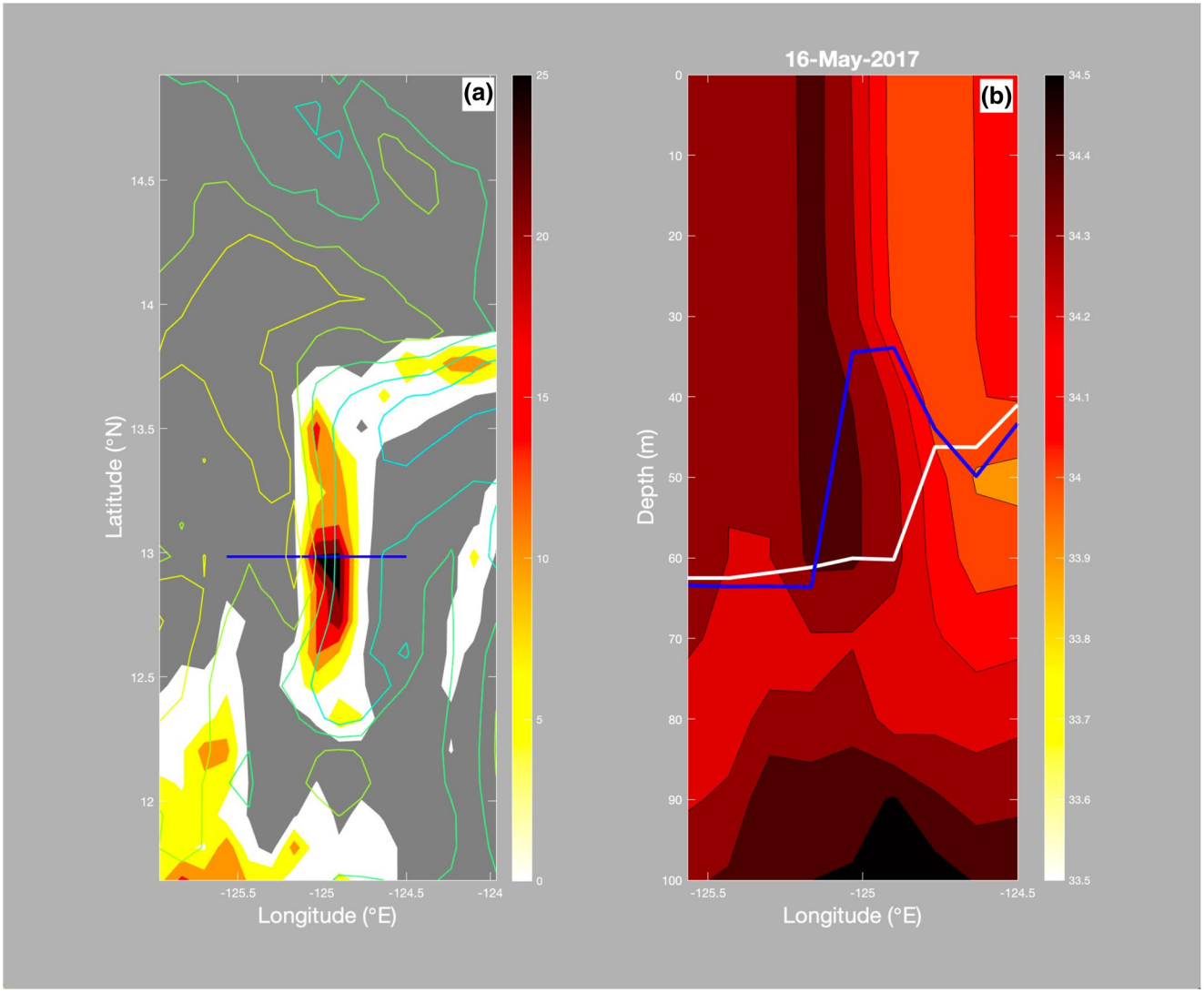

Figure 11. BLT and salinity on May 16, 2017 extracted from Movie S2. (a) Plan view. Colored contours: SSS with contour interval 0.1. High SSS in yellow and low SSS in blue. Colors: BLT with color scale at right. Gray color indicates zero BLT. Blue line is the location of the vertical section displayed in the right panel. (b) Vertical salinity section across the front in the left panel. Blue line is the ILD. White line is the MLD. The difference between them is the BLT. BLT, barrier layer thickness; ILD, isothermal layer depth; MLD, mixed-layer depth; SSS, sea surface salinity.

front near the surface, but tilts through the front to the fresh side with depth (Figure 12a), with the strongest convergence being at the front base at a depth of 60–70 m. The vertical velocity (Figure 11c) has upwelling (red color) just below the surface decreasing to zero at the surface on the fresh side of the front indicating surface divergence. On the opposite side of the front there is downwelling below the surface (blue color) decreasing to zero at the surface indicating surface convergence (Figure 13). At the base of the ML, the sense of change of vertical motion changes, implying convergence at the base of the ML on the fresh side of the front and divergence on the salty side. It should also be noted that no rainfall fell anywhere near the location of this front in this time period, and that examination of the distribution indicated no strong front in temperature as there is in salinity. The temperature difference between the salty and fresh side of the front is at most ~0.1–0.2°C, with the salty side being colder.

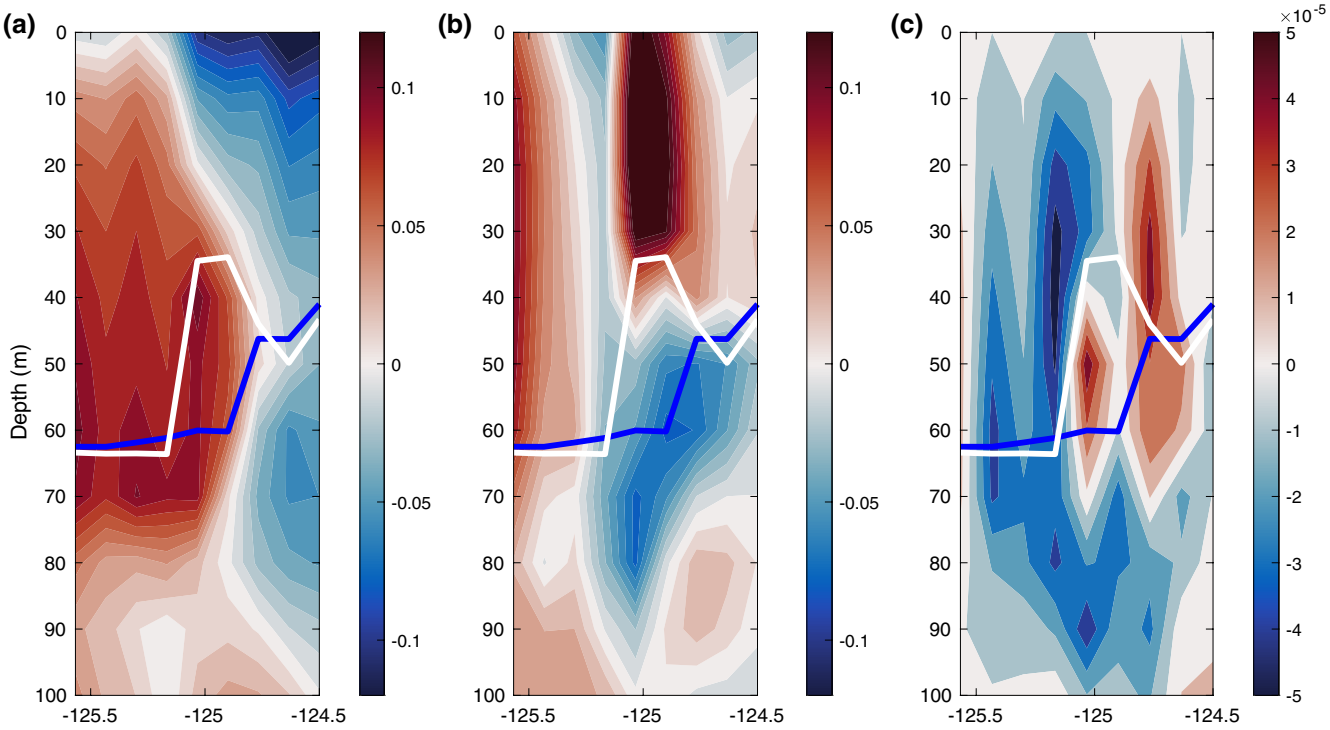

Figure 12. a) Zonal velocity (m/s) along the same section as in Figure 11 right panel for May 16, 2017. White line is the MLD and blue line is the ILD. Red (blue) colors indicate positive (negative) velocity, or to the left (right) in the section. (b) Same as panel (a), but for meridional velocity. Red (blue) colors indicate flow northward or into the page (southward or out of the page) (c) Same as panel (a) but for vertical velocity. Upward flow in red colors, downward in blue. ILD, isothermal layer depth; MLD, mixed-layer depth.

4. Summary and Discussion

Using a version of ROMS set up for the SPURS-2 region in the eastern tropical Pacific Ocean, we have studied two events when BLs appeared in the model. Both events were associated with sharp mixed layer salinity fronts. The first occurred at 6–7°N in October 2017, and was part of a complex of BLs formed along a large-scale front. The other occurred at 12–13°N in May 2017, at the leading edge of the extension of the eastern Pacific fresh pool. In each case, a thick BL was created when the bottom part of a salinity front tilted toward the fresh side of the front. In the October event, the formation of the BL was associated with spreading of fresh over salty water and motion of the salinity front. In the May event, the front remained relatively stationary and persisted for more than 2 weeks.

The hypothesis of KS20 and CM02 is that BLs can be formed by tilting of vertically oriented isohalines by shear flow at a mixed layer salinity front. The analysis of the May and October events suggests a modified version of this mechanism (Figure 14) that the full concurrent property and velocity fields from the model simulation enable us to better resolve compared to in situ observations. This starts with a vertical front of salinity in the mixed layer. On the fresh side of the front, the flow is horizontally divergent at the surface and pulls water up from the mixed-layer base. On the salty side of the front, the flow is convergent at the surface and pushes water down into the mixed layer. The opposite is the case at the base of the mixed layer, with divergence on the salty side and convergence on the fresh side. Thus, a small vertical circulation cell is set up with water flowing across the front at the mixed layer base from the salty to the fresh side. At the base of the mixed layer, the isohalines then tilt generating the BL that is observed. The mixed layer front is accompanied by a strong vertical shear through the thermal wind relation. This vertical shear may play a role in generating and maintaining the horizontal convergences and divergences that drive the vertical circulation (KS20). In particular, the surface divergence on the fresh side of the front may be due to acceleration of the flow by concentration of the front's isohalines at the location of the BL (Figure 12b).

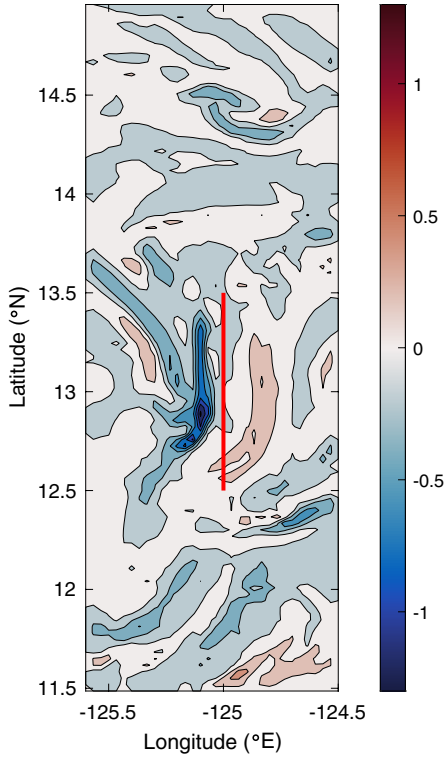

Figure 13. Surface divergence on May 16, 2017. Units are 10^{-5} s^{-1} with color scale at right. A vertical red line indicates the approximate position of the sharpest part of the SSS front in Figure 11. SSS, sea surface salinity.

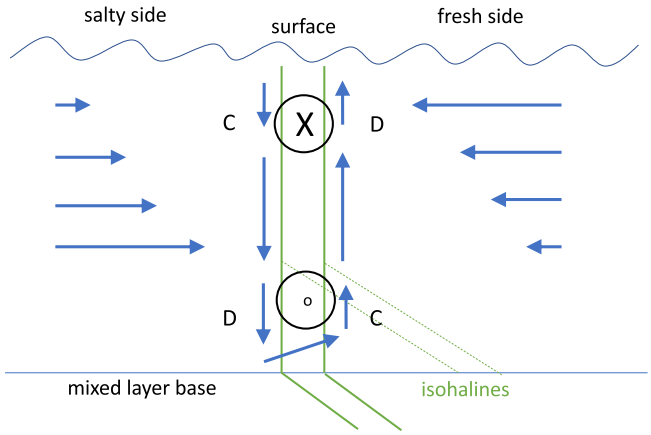

Figure 14. Schematic view of proposed BL formation mechanism in the ETP showing a section across a zonal salinity front in the mixed layer as in Figure 11b. The zonal velocity, the arrows at the left and right, indicate a tilting shear flow. On the salty side of the front there is horizontally convergent flow at the surface and divergent flow at the base of the mixed layer. By contrast, on the fresh side there is divergent flow at the surface and convergent flow at the base of the mixed layer. This sets up a vertical circulation that acts to tilt isohalines mainly at the front's base (dashed lines) and generate a thick BL. Included is a strong vertical shear parallel to the front (into/out of the page) which helps to maintain the vertical orientation of the front at the surface and contribute to the convergent and divergent parts of the flow. BL, barrier layer; ETP, eastern tropical North Pacific.

CM02 postulated that a strong salinity gradient can generate a shear flow across the front and tilt the isohalines in the absence of other processes that might balance the pressure gradient. Perhaps, there are other processes occurring at the surface (e.g., turbulent mixing or wind stress) that can balance the pressure gradient keeping the front vertical there, but not at the base of the mixed layer. Maybe the front itself generates along-front vertical shear (Figure 12b) as it forms through the thermal wind relation which is able to balance the across-front pressure gradient near the surface but not as much at the mixed layer base. The front shown in Figure 11 is there for a long enough time to become geostrophically balanced, and so the thermal wind relation holds there, and the across-front shear is much stronger near the surface than at the mixed layer base (Figure 12a).

The proposed mechanism shown in Figure 14 is two-dimensional. However, it greatly simplifies the mesoscale surface circulation that in reality generates and moves the front and associated convergence/divergence, and it ignores mixing and entrainment of salt through the base of the mixed layer. The schematic does however, place emphasis on vertical processes in the vicinity of a front, which seems appropriate given the apparent association between BL formation, horizontal divergence and the presence of fronts (KS20). Indeed, Vialard and Delecluse (1998b) suggest a similar mechanism, including downwelling near the front, but emphasize the role of precipitation to a greater degree. That study was conducted in the western tropical Pacific where precipitation may be more important in the BL formation process.

KS20 emphasize the importance of Ekman transport in the formation of BLs, especially in summer and fall in the ETP. We note that formation of thick BLs in the October event is associated with a sudden relaxation of the winds between 26 and 27-October (Figures 7b and 7c). There is no indication that the currents slowed or stopped as a result of this (Figure 4). However, the disturbance in the wind forcing may have been enough to produce submesoscale eddies (Thomas et al., 2008), and a growing set of convergences and divergences at the surface (Figure 5) that were able to generate fronts and BLs during October 2017 (see also Movie S1, 18–31 October 2017).

Tanguy et al. (2010) discuss the diversity of situations and causes responsible for the BLs observed in the tropical Atlantic. Some instances of BLs arise in similar ways to those depicted here in the ETP, on the fresh side of a mixed layer salinity front and at the front's base (see their Figures 11c, 11e, and 11f). As noted above, it has been hypothesized that BLs act to insulate the full mixed layer from surface buoyancy flux and entrainment cooling from below (Godfrey & Lindstrom, 1989; Vialard & Delecluse, 1998a) and concentrate heating into the upper part of the mixed layer. If this is the case, then it follows that in the tropics, as these BLs are formed, heating preferentially occurs on the fresh sides of submesoscale fronts. As the mixed layer is heated in that region, the density contrast across the front is enhanced, along with the lifetime of the front. This may be why these fronts can last for long periods of time, such as the one in the Movie S2 which lasts more than 2 weeks, despite the fact that they are unstable. A counterpoint to this is the fact that strong gradients in SST never develop in the two instances where SSS fronts are studied, which we would have expected in the event of differential heating.

In this work, we have analyzed two very limited appearances of BLs and attributed certain characteristics to them. This is not to say that all, or even most, BLs in the ETP necessarily follow this script. However, given the ubiquity of these features as seen in Movie S1 and documented by KS20, there is no doubt the BLs introduce variance into the processes of entrainment at the base of the mixed layer and the flux of heat and fresh water across the surface. This variance itself may help to generate the submesoscale flows that create fronts (Thomas et al, 2008) and in turn work to increase variance in salinity, a positive feedback loop. This positive feedback, acting on the large scale salinity field can perhaps lead to or accelerate the extension of the surface salinity minimum that stretches across the tropical Pacific during the summer and fall (Melnichenko et al., 2019).

Data Availability Statement

SPURS-2 central mooring data can be accessed here: http://dx.doi.org/10.5067/SPUR2-MOOR1. The authors express their appreciation to J. T. Farrar for providing this high quality dataset. SPURS-2 uCTD data can be accessed here: http://dx.doi.org/10.5067/SPUR2-UCTD0. ROMS output can be accessed here: http://dx.doi.org/10.15139/S3/UNJ8FX

Acknowledgments
Color scales for all color figures were taken from the "cmocean" package (Thyng et al., 2016). There are no known financial conflicts of interest on the parts of the authors of this study, neither are there any unstated affiliations among the authors that could be perceived as a conflict of interest. FB's work on SPURS-2 is supported by NASA grant NNX15AF72G, and by the Jet Propulsion Laboratory through the Salinity Continuity Processing activity. SK is supported the Japan Society for the Promotion of Science (JSPS) under its Overseas Research Fellowships program. JS and SK are supported by NASA Grant Number 80NSSC18K1500. We wish to thank two anonymous reviewers, who read the manuscript carefully and provided insightful comments.

References

Alory, G., Maes, C., Delcroix, T., Reul, N., & Illig, S. C. C. (2012). Seasonal dynamics of sea surface salinity off Panama: The far Eastern Pacific Fresh Pool. *Journal of Geophysical Research*, *117*(C4), C04028. https://doi.org/10.1029/2011JC007802

Cronin, M. F., & McPhaden, M. J. (2002). Barrier layer formation during westerly wind bursts. *Journal of Geophysical Research*, *107*(C12), 18020. https://doi.org/10.1029/2001JC00117

de Boyer Montegut, C., Mignot, J., Lazar, A., & Cravatte, S. (2007). Control of salinity on the mixed layer depth over the world ocean: 1. General description. *Journal of Geophysical Research*, *C112*, 6011. https://doi.org/10.1029/2006JC003953

Fairall, C. W., Bradley, E. F., Hare, J., Grachev, A. A., & Edson, J. B. (2003). Bulk parameterization on air–sea fluxes: Updates and verification for the COARE algorithm. *Journal of Climate*, *16*, 571–591.

Farrar, J. T. (2019). *SPURS-2 Central mooring CTD, surface flux and meteorological data for the E. Tropical Pacific field campaign*. Pasadena, CA: NASA/JPL/PO.DAAC. https://doi.org/10.5067/SPUR2-MOOR1

Farrar, J. T., & Plueddemann, A. J. (2019). On the factors driving upper-ocean salinity variability at the western edge of the eastern Pacific fresh pool. *Oceanography*, *32*, 30–39. https://doi.org/10.5670/oceanog.2019.209

Fiedler, P. C., & Talley, L. D. (2006). Hydrography of the eastern tropical Pacific: A review. *Progress in Oceanography*, *69*(2), 143–180. https://doi.org/10.1016/j.pocean.2006.03.008

Godfrey, J. S., & Lindstrom, E. J. (1989). The heat budget of the equatorial western Pacific surface mixed layer. *Journal of Geophysical Research*, *94*(C6), 8007–8017. https://doi.org/10.1029/JC094iC06p08007

Good, S. A., Martin, M. J., & Rayner, N. A. (2013). EN4: Quality controlled ocean temperature and salinity profiles and monthly objective analyses with uncertainty estimates. *Journal of Geophysical Research: Oceans*, *118*(12), 6704–6716. https://doi.org/10.1002/2013JC009067

Guimbard, S., Reul, N., Chapron, B., Umbert, M., & Maes, C. (2017). Seasonal and interannual variability of the Eastern Tropical Pacific Fresh Pool. *Journal of Geophysical Research: Oceans*, *122*(3), 1749–1771. https://doi.org/10.1002/2016JC012130

Katsura, S., Oka, E., & Sato, K. (2015). Formation mechanism of barrier layer in the subtropical Pacific. *Journal of Physical Oceanography*, *45*(11), 2790–2805. https://doi.org/10.1175/JPO-D-15-0028.1

Katsura, S., & Sprintall, J. (2020). Seasonality and formation of barrier layers and associated temperature inversions in the Eastern Tropical North Pacific. *Journal of Physical Oceanography*, *50*(3), 791–808. https://doi.org/10.1175/JPO-D-19-0194.1

Katsura, S., Sprintall, J., & Bingham, F. M. (2020). Upper ocean stratification in the eastern Pacific during the SPURS-2 field campaign. https://doi.org/10.1002/essoar.10504779.1

Li, Z. (2020). *SPURS-2 ROMS 1-Feb-2017—31-Jan-2018*. https://doi.org/10.15139/S3/UNJ8FX

Li, Z., Bingham, F. M., & Li, P. P. (2019). Multiscale simulation, data assimilation, and forecasting in support of the SPURS-2 field campaign. *Oceanography*, *32*, 131–141. https://doi.org/10.5670/oceanog.2019.221

Li, Z., McWilliams, J. C., Ide, K., & Farrara, J. D. (2015). A multiscale variational data assimilation scheme: Formulation and illustration. *Monthly Weather Review*, *143*(9), 3804–3822. https://doi.org/10.1175/MWR-D-14-00384.1

Lindstrom, E. J., Edson, J. B., Schanze, J. J., & Shcherbina, A. Y. (2019). SPURS-2: Salinity processes in the upper-ocean regional study 2—The eastern equatorial Pacific experiment. *Oceanography*, *32*, 15–19. https://doi.org/10.5670/oceanog.2019.207

Lukas, R., & Lindstrom, E. (1991). The mixed layer of the western equatorial Pacific. *Journal of Geophysical Research*, *96*(suppl), 3343–3357. https://doi.org/10.1029/90JC01951

Maes, C., Picaut, J., & Belamari, S. (2002). Salinity barrier layer and onset of El Niño in a Pacific coupled model. *Geophysical Research Letters*, *29*(24), 5951–5954. https://doi.org/10.1029/2002GL016029

Maes, C., Picaut, J., & Belamari, S. (2005). Importance of the salinity barrier layer for the buildup of El Niño. *Journal of Climate*, *18*(1), 104–118. https://doi.org/10.1175/JCLI-3214.1

Melnichenko, O., Hacker, P., Bingham, F. M., & Lee, T. (2019). Patterns of SSS variability in the eastern tropical Pacific: Intraseasonal to interannual timescales from seven years of NASA satellite data. *Oceanography*, *32*, 20–29. https://doi.org/10.5670/oceanog.2019.208

Pujol, M. I., Faugère, Y., Taburet, G., Dupuy, S., Pelloquin, C., Ablain, M., & Picot, N. (2016). DUACS DT2014: The new multi-mission altimeter data set reprocessed over 20 years. *Ocean Science*, *12*(5), 1067–1090. https://doi.org/10.5194/os-12-1067-2016

Qu, T., Song, Y. T., & Maes, C. (2014). Sea surface salinity and barrier layer variability in the equatorial Pacific as seen from Aquarius and Argo. *Journal of Geophysical Research: Oceans*, *119*, 15–29. https://doi.org/10.1002/2013JC009375

Roemmich, D., Morris, M., Young, W. R., & Donguy, J. R. (1994). Fresh equatorial jets. *Journal of Physical Oceanography*, *24*(3), 540–558. https://doi.org/10.1175/1520-0485(1994)024<0540:FEJ>2.0.CO;2

Rutledge, S. A., Chandrasekar, V., Fuchs, B., George, J., Junyent, F., Kennedy, P., & Dolan, B. (2019). Deployment of the SEA-POL C-band polarimetric radar to SPURS-2. *Oceanography*, *32*(2), 50–57. https://doi.org/10.5670/oceanog.2019.212

Sato, K., Suga, T., & Hanawa, K. (2004). Barrier layer in the North Pacific subtropical gyre. *Geophysical Research Letters*, *31*, 5301. https://doi.org/10.1029/2003GL018590

Sato, K., Suga, T., & Hanawa, K. (2006). Barrier layers in the subtropical gyres of the world's oceans. *Geophysical Research Letters*, *33*, L08603. https://doi.org/10.1029/2005GL025631

Schanze, J. J., Schmitt, R. W., & Yu, L. L. (2010). The global oceanic freshwater cycle: A state-of-the-art quantification. *Journal of Marine Research*, *68*(3–1), 569–595. https://doi.org/10.1357/002224010794657164

Shchepetkin, A. F., & McWilliams, J. C. (2011). Accurate Boussinesq oceanic modeling with a practical, stiffened equation of state. *Ocean Modelling*, *38*, 41–70.

Sprintall, J. (2019a). *SPURS-2 research vessel underway CTD (uCTD) data for the E. Tropical Pacific R/V Revelle cruises. Ver. 1.0*. PO.DAAC, CA, USA. https://doi.org/10.5067/SPUR2-UCTD0

Sprintall, J. (2019b). Upper ocean salinity stratification during SPURS-2. *Oceanography*, *32*(2), 40–41. https://doi.org/10.5670/oceanog.2019.210

Sprintall, J., & Tomczak, M. (1992). Evidence for the barrier layer in the surface layer of the tropics. *Journal of Geophysical Research*, *97*, 7305–7316. https://doi.org/10.1029/92JC00407

Tanguy, Y., Arnault, S., & Lattes, P. (2010). Isothermal, mixed, and barrier layers in the subtropical and tropical Atlantic Ocean during the ARAMIS experiment. *Deep Sea Research Part I: Oceanographic Research Papers*, *57*(4), 501–517. https://doi.org/10.1016/j.dsr.2009.12.012

Thomas, L. N., Tandon, A., & Mahadevan, A. (2008). Sub-mesoscale processes and dynamics. In M. W. Hecht, & H. Hasumi (Eds.), *Ocean modeling in an Eddying regime, Geophysical Monograph Series 177* (pp. 17–38). Washington, DC: American Geophysical Union.

Thompson, E. J., Asher, W. E., Jessup, A. T., & Drushka, K. (2019). High-resolution rain maps from an X-band marine radar and their use in understanding ocean freshening. *Oceanography*, *32*(2), 58–65. https://doi.org/10.5670/oceanog.2019.213

Thyng, K. M., Greene, C. A., Hetland, R. D., Zimmerle, H. M., & DiMarco, S. F. (2016). True colors of oceanography: Guidelines for effective and accurate colormap selection. *Oceanography*, *29*(3), 9–13. https://doi.org/10.5670/oceanog.2016.66

Veneziani, M., Griffa, A., Garraffo, Z., & Mensa, J. A. (2014). Barrier layers in the tropical South Atlantic: Mean dynamics and submesoscale effects. *Journal of Physical Oceanography*, *44*(1), 265–288. https://doi.org/10.1175/JPO-D-13-064.1

Vialard, J., & Delecluse, P. (1998a). An OGCM study for the TOGA decade. Part I: Role of salinity in the physics of the Western Pacific fresh pool. *Journal of Physical Oceanography*, *28*(6), 1071–1088. https://doi.org/10.1175/1520-0485(1998)028<1071:AOSFTT>2.0.CO;2

Vialard, J., & Delecluse, P. (1998b). An OGCM study for the TOGA decade. Part II: Barrier-layer formation and variability. *Journal of Physical Oceanography*, *28*(6), 1089–1106. https://doi.org/10.1175/1520-0485(1998)028%3C1089:AOSFTT%3E2.0.CO;2

Yu, L. (2015). Sea-surface salinity fronts and associated salinity-minimum zones in the tropical ocean. *Journal of Geophysical Research: Oceans*, *120*, 4205–4225. https://doi.org/10.1002/2015JC010790